Proceedings of the ASME 2020
Dynamic Systems and Control Conference
DSCC2020
October 4-7, 2020, Pittsburgh, PA, USA

DSCC2020-3219

TRAFFIC PREDICTION FOR MERGING COORDINATION CONTROL IN MIXED TRAFFIC SCENARIOS

Yunli Shao*, Jackeline Rios-Torres
Energy and Transportation Science Division,
Oak Ridge National Laboratory, Oak Ridge, TN 37831

ABSTRACT

Connected and autonomous vehicles (CAVs) have the potential to bring in safety, mobility, and energy benefits to transportation. The control decisions of CAVs are usually determined for a look-ahead horizon based on previewed traffic information. This requires an effective prediction of future traffic conditions and its integration with the CAV control framework. However, the short-term traffic prediction using information from connectivity is a challenging research topic, especially for mixed traffic scenarios. This work focuses on the development of a traffic prediction framework for a merging coordination controller. The previously developed merging controller coordinates the merging sequence and travel speed of CAVs to maximize the energy efficiency and overall mobility. In mixed traffic scenarios, the controller receives information regarding the position of all the vehicles traveling inside a control zone and controls the desired speed of all CAVs. The controller has no control on the human-driven vehicles. The merging controller does not have direct information or an explicit prediction on the behaviors of human-driven vehicles. Aiming to improve the performance of the merging controller in various mixed traffic conditions, a traffic prediction algorithm is developed and evaluated in this work. The performance of this traffic prediction algorithm is investigated for various penetration rates of connectivity for a single-lane secondary road merging to a single-lane primary road. The results show that compared to a constant speed assumption of human-driven vehicles, the proposed traffic prediction algorithm is able to reduce the prediction error of the arrival time of human-driven vehicles at the merging zone by more than 50%.

Keywords: Connected and autonomous vehicle, cooperative merging, optimal merging coordination, traffic prediction

1. INTRODUCTION

Connected and autonomous vehicles (CAVs) have the potential to benefit safety, mobility, and energy aspects of transportation systems [1]. Connectivity enables vehicle-to-vehicle and vehicle-to-infrastructure communication, allowing vehicles to have access to real-time information not available before. Such information includes preceding vehicles' location and speed, signal phase and timing, road curvature and slope angles, etc. In addition, full or partial automation enables precise control of vehicle speed and acceleration. The information brought by connectivity and on-board sensors of automated vehicles provides an opportunity to effectively predict the future traffic conditions. Therefore, CAVs can be proactively controlled based on the previewed information in an optimal fashion. Control decisions of CAVs are usually determined for a look-ahead horizon based on predicted traffic information. For example, when approaching a signalized intersection with broadcast SPaT information, a CAV can adjust its vehicle speed and arrival time to pass the intersection without braking and idling [2,3]. When following other vehicles with broadcast vehicle information, a CAV can anticipate slowdowns and

* Contact author: shaoy@ornl.gov

maintain a steady and smooth vehicle speed profile [4,5]. In these example applications, an optimization problem is usually solved to minimize a particular cost function, such as control effort, energy consumption, travel time, etc., for an upcoming time horizon [6–9]. Thus, it becomes apparent that the integration of traffic prediction algorithms with optimal control frameworks for CAVs is critical to achieve more effective control.

The traffic prediction discussed here is short-term covering prediction for tens of seconds in the future [3]. The prediction horizon has to be determined considering the benefits from optimal control and accuracy of prediction, which will vary according to each specific CAV application. It is ideal to have a long preview horizon to maximize the benefits from the CAV optimization. However, usually the longer the horizon, the lower the accuracy [10], particularly when human drivers are involved given their unknown and uncertain behaviors. In literature, researchers [11,12] have developed short-term prediction of individual driver's behavior using information of an immediate preceding vehicle (e.g. from radar system). While it is possible to obtain reasonable predictions for very short time horizons (few seconds in the future), it is challenging to provide accurate prediction for longer time horizons. This is because a driver's behavior is uncertain in nature and depends on the traffic conditions in front of it. Connectivity enables access to the current status of vehicles in front of a vehicle, thus making it possible for both drivers and CAV controllers to preview upcoming traffic conditions to plan ahead their maneuvers.

There have been some preliminary work focused on how to use the information from connectivity to anticipate short-term future traffic conditions [13,14]. In these studies, it is typically assumed that all vehicles on the road are connected. This corresponds to an ideal case and there will be a transitional period where human-driven non-connected vehicles will share the road with connected and/or automated vehicles [15]. Such mixed traffic scenario brings additional challenges for traffic prediction since there is no direct information regarding the behavior of human-driven vehicles. The uncertain behavior of the human-driven vehicles can significantly affect the performance of CAVs [16–18]. It is critical to integrate traffic prediction algorithms with optimal control frameworks for CAVs to achieve a more effective control.

Generally, traffic models can be divided into two categories [19]: microscopic models and macroscopic models. Microscopic models describe each individual vehicle's behavior explicitly and have been widely implemented in many traffic simulator software [20]. It is challenging to model behaviors of human-driven vehicles in a real-time CAV application due to lack of direct information. In addition, microscopic models may become computationally intractable as the complexity of the traffic network and the number of vehicles increase. Macroscopic models [21,22] describe the vehicle stream as a whole and uses traffic characteristics that are analog to a fluid stream, such as flow, density, and flow speed. Therefore, these models can be readily applied to mixed-traffic scenarios [23,24]. Another advantage of macroscopic-level modeling is the ability to capture traffic bottlenecks which fundamentally affect the behavior of vehicles. The bottlenecks refer to any roadway features that will alter or constrain the traffic such as traffic signal light, on-ramp/off-ramp, lane closure, etc. Modeling the bottlenecks is crucial for predicting more than next few seconds. With the emerging of data-driven models, researchers have studied both data based microscopic and macroscopic traffic prediction models [25–27]. Data-driven models usually require lots of real-world data to calibrate and train the model, which is not trivial given the challenges in obtaining and calibrating the data from heterogeneous sources.

Considering the challenges and the advantage of using traffic prediction for effective CAV control, the contribution of this work is the development of a traffic prediction framework for a merging coordination application under a mixed traffic scenario. In this scenario, the merging controller receives information regarding the position of all vehicles traveling inside a control zone. The controller coordinates the vehicle arrival time at the merging zone and controls the desired speed of all CAVs. The controller has no control on the human-driven vehicles. The merging coordination controller developed in previous work [9] assumes the human-driven vehicles travel at constant speed within the control zone to anticipate their arrival time at the merging zone (see Figure 1). This assumption works in light traffic conditions but may not always hold for dense traffic scenarios. Therefore, the motivation of this work is to develop a traffic prediction algorithm that can be later integrated into the merging coordination control for various traffic scenarios. Note that this work focuses on the development of the traffic prediction algorithm but the integration of the traffic prediction with the merging coordination control is part of the future work. The performance of the traffic prediction algorithm is investigated for various penetration rates of connectivity for a single-lane secondary road merging to a single-lane primary road (see Figure 1), but the proposed prediction algorithm has the potential to be extended to more complex merging scenarios.

The remainder of the paper is organized as follows: Section 2 formulates the traffic prediction framework; Section 3 evaluates the proposed traffic prediction in various traffic scenarios and finally, Section 4 concludes the paper.

2. TRAFFIC PREDICTION FRAMEWORK

The traffic around the merging area is modeled as a dynamical system based on the traffic flow model (see Figure 1). The underlining prediction framework builds upon the work in [3], where a simple single-lane road is considered with no merging and lane-change. As shown in Figure 1, the entire roadway is divided into multiple cells with length dx. The dynamic of each cell is described using two states: density and flow speed. The prediction is updated as new information becomes available. The merging coordination control is implemented in a rolling horizon fashion, i.e., it is updated at each control time step. At every update instance, information regarding speed and location is shared by each CAV located inside the control zone. This information provides partial measurement of the traffic states of the cell where the CAV is located. A state estimator (observer) is then applied to estimate

all the rest unknown traffic states for the entire roadway. Once the current traffic states are known, future traffic states are predicted by propagating the traffic model forward in time. Then, the arrival time of the human-driven vehicles at the merging zone is predicted and used as an input to the merging coordination control. The controller [9] will then coordinate the arrival time of all CAVs at the merging zone and optimize their speed.

As shown in Figure 1, the merging zone includes two lanes where vehicles from the acceleration lane changes lane to the merge lane. This require the traffic model to consider multi-lane as well as lane-change behaviors. Typically, traffic flow models are applied to study the overall behavior of the aggregated traffic considering a time scale in the order of minutes and cell length in the order of hundreds of meters. The merging zone is usually considered as a single cell and lane-change behaviors are simplified or neglected. In this work, a detailed merging zone is considered to provide the desired prediction resolution, i.e., the next 10-20 seconds and cell length of 10-20 meters, which is required for the merging coordination control. The lane-change and merging behaviors are considered, and the merging zone is modeled with multiple cells. The traffic prediction framework in this work is applied to a single-lane secondary road merging into a single-lane primary road as a case study. The general concept of the framework can be extended and applied to other merging applications of CAVs, or the modeling and speed prediction of merging control.

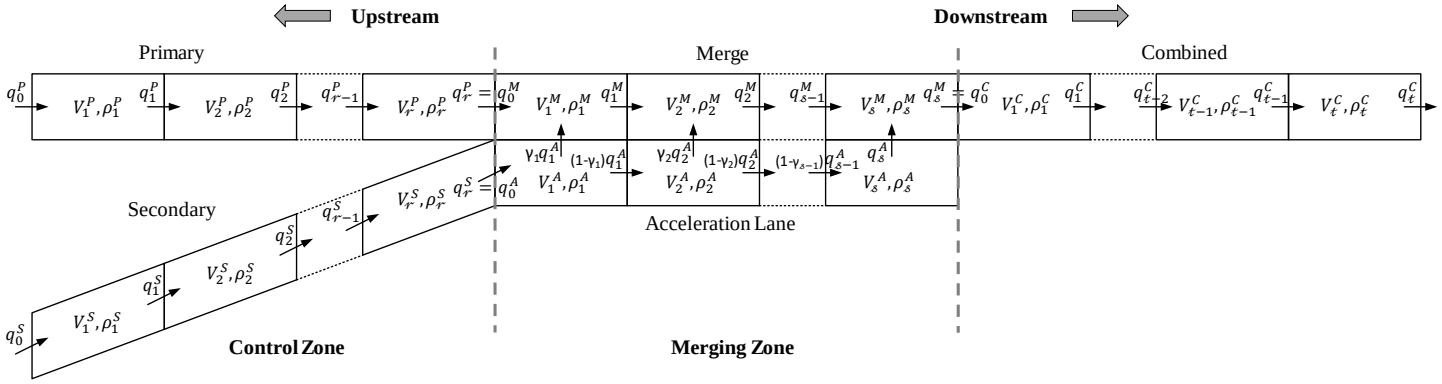

Figure 1 Discretized merging area for traffic modeling

2.1. Traffic model

As shown in Figure 1, the entire roadway around the merging area is modeled and divided into five road segments: primary, secondary, merge, acceleration lane, and combined. It is important to model a segment downstream the merge segment, which is identified as the combined road segment, since its traffic conditions will affect the dynamics inside the merging zone. Any congestion inside the combined road segment will propagate upstream to the merging zone. For primary, secondary and combined road segments, there is only a single-lane with no lane-changing and merging. The dynamic of these segments is described using the same model (Section 2.1.1). For merge and acceleration lane segments, a lane-changing and merging model is developed and applied (Section 2.1.2 and Section 2.1.3). These two road segments have different models as the vehicle can only move from the acceleration lane road segment to the merge road segment but not vice versa. The five road segments are divided into cells of length $dx = 20$ meters. It is assumed that control zones of both primary and secondary road segments have the same total length (400 meters) and are divided into r cells. Merge and acceleration lane road segments have the same length (120 meters) and are divided into s cells. The combined road segment is divided into t cells. The dynamics of each cell j is described using two states: flow speed V_j $(meter/second)$ and density ρ_j $(veh/meter)$. Variable q_j $(veh/second)$ denotes the flow between each cell and the flow equals to traffic speed times traffic density, that is:

$$q_j(k) = \rho_j(k) V_j(k) \tag{1}$$

2.1.1. Primary, secondary, and combined road segments

For each of the primary, secondary, and combined road segments, a stochastic traffic flow model is adopted to describe the dynamics of each cell j. Stochastic model is adopted to facilitate the observer design in Section 2.3. The flow model is given by [3,28]:

$$\rho_j(k+1) = \rho_j(k) + \frac{dt}{dx}\left[q_{j-1}(k) - q_j(k)\right] + \omega_j(k) \tag{2}$$

$$\begin{aligned} V_j(k+1) = V_j(k) &+ \frac{dt}{dx} V_j(k)\left[V_{j-1}(k) - V_j(k)\right] \\ &+ dt \cdot \left[V_e\left(\rho_j(k)\right) - V_j(k)\right]/\tau \\ &- \frac{dt}{dx} \cdot c_0^2 \frac{\left[\rho_{j+1}(k) - \rho_j(k)\right]}{(\rho_j(k) + \epsilon)} + \zeta_j(k) \end{aligned} \tag{3}$$

where (2) is the vehicle conservation equation; (3) describes the traffic speed dynamics; k is the discretized time instance; dt is

the time step (selected as 0.5 seconds); dx is the length of each cell (selected as 20 meters); ϵ is a small value to prevent zero denominator; $\omega_j(k)$ and $\zeta_j(k)$ describe model uncertainties and are assumed to follow stochastic Gaussian distributions. $V_e(\rho_j(k))$ is based on the following fundamental diagram [19]:

$$V_e\left(\rho_j(k)\right) = \begin{cases} \dfrac{(v_c - v_0)}{\rho_c} \cdot \rho_j(k) + v_0 & \rho_j(k) < \rho_c \\ \dfrac{v_c \rho_c}{(\rho_m - \rho_c)} \cdot \left(\dfrac{\rho_m}{\rho_j(k)} - 1\right) & \rho_j(k) \geq \rho_c \end{cases} \quad (4)$$

There are six model parameters: τ is the adaptation rate of the vehicle to reach the speed of the fundamental diagram; c_0 characterizes the impacts of traffic ahead (downstream traffic) on current cell; v_0 is free driving speed; v_c is the vehicle speed at the road capacity; ρ_m is the density when vehicle is stationary; ρ_c is the density at road capacity.

Special treatments are necessary for the boundary cells of each road segment. For the first cell of primary and secondary road segments, it is assumed that the flow coming into the cells can be estimated by loop detector or connected vehicle information. Therefore, $q_0^P(k), V_0^P(k)$ and $q_0^S(k), V_o^S(k)$ are assumed to be known. For the last cell of the primary and secondary road segments, the following relationship holds:

$$\rho_{r+1}^P(k) = \rho_1^M(k), \qquad \rho_{r+1}^S(k) = \rho_1^A(k) \quad (5)$$

For the last cell of the combined road segment, it is assumed that the outflow will be at free driving condition. Therefore, $\rho_{t+1}^C(k)$ is known. For the first cell of the combined road segment, the following relationship holds:

$$q_0^C(k) = q_s^M(k), \qquad V_0^C(k) = V_s^M(k) \quad (6)$$

The state equation for primary road segment includes total of r cells. The dynamic of each cell is described using (2)(3). The dynamic of the entire primary road segment can be concisely written as:

$$\boldsymbol{x}^P(k+1) = f^P(\boldsymbol{x}^P(k), \boldsymbol{\omega}^P(k), \boldsymbol{\zeta}^P(k)) \quad (7)$$

where f^P denotes the functions in (2), (3), and vector $\boldsymbol{x}^P(k), \boldsymbol{\omega}^P(k), \boldsymbol{\zeta}^P(k)$ are described by:

$$\boldsymbol{x}^P(k) = [\rho_1^P \quad \rho_2^P \quad \cdots \quad \rho_r^P \quad V_1^P \quad V_2^P \quad \cdots \quad V_r^P] \quad (8)$$

$$\boldsymbol{\omega}^P(k) = [\omega_1^P \quad \omega_2^P \quad \cdots \quad \omega_r^P] \quad (9)$$

$$\boldsymbol{\zeta}^P(k) = [\zeta_1^P \quad \zeta_2^P \quad \cdots \quad \zeta_r^P] \quad (10)$$

Similarly, for the secondary road segment there are total of r cells, thus the state equation can be denoted as:

$$\boldsymbol{x}^S(k+1) = f^S(\boldsymbol{x}^S(k), \boldsymbol{\omega}^S(k), \boldsymbol{\zeta}^S(k)) \quad (11)$$

$$\boldsymbol{x}^S(k) = [\rho_1^S \quad \rho_2^S \quad \cdots \quad \rho_r^S \quad V_1^S \quad V_2^S \quad \cdots \quad V_r^S] \quad (12)$$

$$\boldsymbol{\omega}^S(k) = [\omega_1^S \quad \omega_2^S \quad \cdots \quad \omega_r^S] \quad (13)$$

$$\boldsymbol{\zeta}^S(k) = [\zeta_1^S \quad \zeta_2^S \quad \cdots \quad \zeta_r^S] \quad (14)$$

For the combined road segment there are a total of t cells, thus the state equation can be denoted as:

$$\boldsymbol{x}^C(k+1) = f^C(\boldsymbol{x}^C(k), \boldsymbol{\omega}^C(k), \boldsymbol{\zeta}^C(k)) \quad (15)$$

$$\boldsymbol{x}^C(k) = [\rho_1^C \quad \rho_2^C \quad \cdots \quad \rho_t^C \quad V_1^C \quad V_2^C \quad \cdots \quad V_t^C] \quad (16)$$

$$\boldsymbol{\omega}^C(k) = [\omega_1^C \quad \omega_2^C \quad \cdots \quad \omega_t^C] \quad (17)$$

$$\boldsymbol{\zeta}^C(k) = [\zeta_1^C \quad \zeta_2^C \quad \cdots \quad \zeta_t^C] \quad (18)$$

2.1.2. Acceleration lane road segment

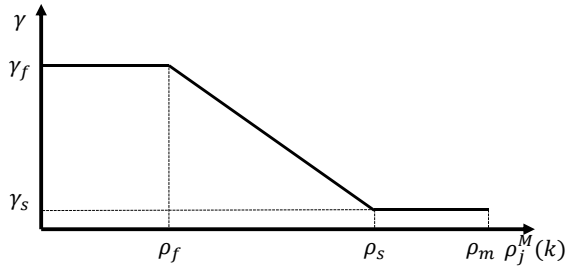

Figure 2 Model of the merging flow ratio

In the acceleration lane, at each cell, part of the traffic flow will enter the adjacent cell of the merge road segment (lane-change), and part of the traffic flow will continue to the next cell of the acceleration lane. The model of this lane-change and merging behavior is based on the observation that drivers are more likely to change lane to the merge segment if the traffic in merge segment is lighter, i.e., if the density in the merge road segment is low. Therefore, the ratio of the traffic flow moving to the adjacent cell in the merge road segment is described as a function of the density of the cell as represented in Figure 2. Mathematically, the traffic flow model of the acceleration lane road segment is described by:

$$\rho_j^A(k+1) = \rho_j^A(k) + \frac{dt}{dx}\left[(1-\gamma_{j-1}(k))q_{j-1}^A(k) - q_j^A(k)\right] + \omega_j^A(k) \quad (19)$$

$$V_j^A(k+1) = V_j^A(k) + \frac{dt}{dx}V_j^A(k)\left[V_{j-1}^A(k) - V_j^A(k)\right] + dt \cdot \left[V_e\left(\rho_j^A(k)\right) - V_j^A(k)\right]/\tau - \frac{dt}{dx} \cdot c_0^2 \frac{\left[\rho_{j+1}^A(k) - \rho_j^A(k)\right]}{(\rho_j^A(k) + \epsilon)} + \zeta_j^A(k) \quad (20)$$

$$\gamma_j(k) = min\left(\gamma_f, max\left(k_\alpha \cdot \rho_j^M(k) + b_\alpha, \gamma_s\right)\right) \quad (21)$$

$$k_\gamma = \frac{\gamma_f - \gamma_s}{\rho_f - \rho_s}, \; b_\gamma = -\frac{\gamma_f - \gamma_s}{\rho_f - \rho_s} \cdot \rho_s + \gamma_s \quad (22)$$

where the variable symbols and model parameters follow the description in Section 2.1.1. There are four additional model parameters which describe the merging ratio $\gamma_j(k)$ of each cell (see Figure 2): γ_f is the ratio at free flow; γ_s is the ratio at saturation flow (congestion); ρ_f is the turnaround density of free flow ratio; ρ_s is the turnaround density of the saturation flow ratio.

For the first cell of the acceleration lane:

$$q_0^A(k) = q_r^S(k), \qquad V_0^A(k) = V_r^S(k), \qquad \gamma_0(k) = 0 \quad (23)$$

For the last cell of the acceleration lane:

$$\rho_{s+1}^{A}(k) = \rho_{s}^{M}(k) \tag{24}$$

The acceleration lane road segment has total of s cells. The state equation can be denoted as

$$\boldsymbol{x}^{A}(k+1) = f^{A}(\boldsymbol{x}^{A}(k), \boldsymbol{\omega}^{A}(k), \boldsymbol{\zeta}^{A}(k)) \tag{25}$$

$$\boldsymbol{x}^{A}(k) = [\rho_1^A \quad \rho_2^A \quad \cdots \quad \rho_s^A \quad V_1^A \quad V_2^A \quad \cdots \quad V_s^A] \tag{26}$$

$$\boldsymbol{\omega}^{A}(k) = [\omega_1^A \quad \omega_2^A \quad \cdots \quad \omega_s^A] \tag{27}$$

$$\boldsymbol{\zeta}^{A}(k) = [\zeta_1^A \quad \zeta_2^A \quad \cdots \quad \zeta_s^A] \tag{28}$$

2.1.3. Merge road segment

For each cell of the merge road segment, the input traffic flow includes the flow from the previous merge road cell and the merge-in flow from the adjacent cell of the acceleration lane. In addition, due to the difference in the flow speed of acceleration lane and the merge road segments, the merge-in flow will create a transient in the flow speed of the merge road cell. This is modeled using an additional lane-change acceleration term $a_j^{\ell}(k)$. The dynamic model is defined by:

$$\begin{aligned}\rho_j^M(k+1) = {} & \rho_j^M(k) \\ & + \frac{dt}{dx}\left[q_{j-1}^M(k) - q_j^M(k) + \gamma_j(k) q_j^A(k)\right] + \omega_j^M(k)\end{aligned} \tag{29}$$

$$\begin{aligned}V_j^M(k+1) = {} & V_j^M(k) + \frac{dt}{dx} V_j^M(k)\left[V_{j-1}^M(k) - V_j^M(k)\right] \\ & + dt \cdot \left[V_e\left(\rho_j^M(k)\right) - V_j^M(k)\right]/\tau \\ & - \frac{dt}{dx} \cdot \frac{c_0^2\left[\rho_{j+1}^M(k) - \rho_j^M(k)\right]}{\left(\rho_j^M(k) + \epsilon\right)} + a_j^{\ell}(k) + \zeta_j^M(k)\end{aligned} \tag{30}$$

$$a_j^{\ell}(k) = \frac{q_j^A(k)\left(V_j^A(k) - V_j^M(k)\right)}{\rho_j^M(k) + \epsilon} \tag{31}$$

All the model parameters follow the previous definitions in Section 2.1.1 and Section 2.1.2.

For the first cell of the merge road segment:

$$q_0^M(k) = q_r^P(k), \qquad V_0^M(k) = V_r^P(k) \tag{32}$$

For the last cell of the merge road segment:

$$\rho_{s+1}^M(k) = \rho_1^C(k) \tag{33}$$

The merge road segment has total of s cells. The state equation can be denoted as:

$$\boldsymbol{x}^{M}(k+1) = f^{M}(\boldsymbol{x}^{M}(k), \boldsymbol{\omega}^{M}(k), \boldsymbol{\zeta}^{M}(k)) \tag{34}$$

$$\boldsymbol{x}^{M}(k) = [\rho_1^M \quad \rho_2^M \quad \cdots \quad \rho_s^M \quad V_1^M \quad V_2^M \quad \cdots \quad V_s^M] \tag{35}$$

$$\boldsymbol{\omega}^{M}(k) = [\omega_1^M \quad \omega_2^M \quad \cdots \quad \omega_s^M] \tag{36}$$

$$\boldsymbol{\zeta}^{M}(k) = [\zeta_1^M \quad \zeta_2^M \quad \cdots \quad \zeta_s^M] \tag{37}$$

2.1.4. State equation for entire merging area

The state equation for the entire merging area consists of the dynamic model for each of the five road segments. The state equation can be written as

$$\boldsymbol{x}(k+1) = \begin{bmatrix}\boldsymbol{x}^P(k+1)\\ \boldsymbol{x}^S(k+1)\\ \boldsymbol{x}^C(k+1)\\ \boldsymbol{x}^M(k+1)\\ \boldsymbol{x}^A(k+1)\end{bmatrix} = \underbrace{\begin{bmatrix} f^P(\boldsymbol{x}^P(k), \boldsymbol{\omega}^P(k), \boldsymbol{\zeta}^P(k))\\ f^S(\boldsymbol{x}^S(k), \boldsymbol{\omega}^S(k), \boldsymbol{\zeta}^S(k))\\ f^C(\boldsymbol{x}^C(k), \boldsymbol{\omega}^C(k), \boldsymbol{\zeta}^C(k))\\ f^M(\boldsymbol{x}^M(k), \boldsymbol{\omega}^M(k), \boldsymbol{\zeta}^M(k))\\ f^A(\boldsymbol{x}^A(k), \boldsymbol{\omega}^A(k), \boldsymbol{\zeta}^A(k))\end{bmatrix}}_{f(\boldsymbol{x}(k), \boldsymbol{\omega}(k), \boldsymbol{\zeta}(k))} \tag{38}$$

2.2. Measurement model

Real-time information communicated from CAVs provide partial measurement on flow speed of the cells where the CAVs are located. If there are multiple CAVs within the same cell, their averaged speed is considered as the flow speed for that cell. The speed measurement equation is:

$$y_i(k) = V_{j_i}(k) + \delta_i \tag{39}$$

where y_i is the speed measurement of i-th cell (or generally i-th CAV); j_i is the index of the cell; δ_i is the Gaussian random variable to model measurement uncertainties.

Suppose the CAVs provide measurement on a total of g cells among all road segments, the measurement equation can be written as:

$$\boldsymbol{y}(k) = \begin{bmatrix}y_1(k)\\ y_2(k)\\ \vdots\\ y_g(k)\end{bmatrix} = \underbrace{\begin{bmatrix}h_1(\boldsymbol{x}(k), \delta_1(k))\\ h_2(\boldsymbol{x}(k), \delta_2(k))\\ \vdots\\ h_g(\boldsymbol{x}(k), \delta_g(k))\end{bmatrix}}_{\boldsymbol{h}(\boldsymbol{x}(k), \boldsymbol{\delta}(k))} \tag{40}$$

$$\boldsymbol{\delta}(k) = [\delta_1 \quad \delta_2 \quad \cdots \quad \delta_g] \tag{41}$$

2.3. Observer

As partial flow speed is measured by CAVs, the rest unknown traffic states are estimated using an observer. The traffic model in Section 2.1 has several nonlinearities and discontinuities. It is challenging to apply analytical nonlinear observer techniques such as those based on Lipschitz analysis [29,30]. Among other nonlinear observers, Unscented Kalman Filter (UKF) [26,27] is selected. Extended Kalman Filter (EKF) is not considered due to the discontinuities in the model. Particle Filters are not selected due to their potential computational burden. UKF provides a systematic approach to use the partially measured traffic states obtained from CAVs to correct the state estimation from the traffic flow model. The system state equation and measurement equation are (from (38) and (39))

$$\begin{aligned}\boldsymbol{x}(k+1) &= f\left(\boldsymbol{x}(k), \boldsymbol{\omega}(k), \boldsymbol{\zeta}(k)\right) \\ \boldsymbol{y}(k) &= h(\boldsymbol{x}(k), \boldsymbol{\delta}(k))\end{aligned} \tag{42}$$

The total size of the states is $N = 2r + 2s + t$. The standard UKF is applied [31]. The procedure of UKF is briefly summarized here and a detailed description can be found in [26,28]. First, calculate a priori state estimation $\hat{\boldsymbol{x}}^{-}(k)$ and covariance estimation $\boldsymbol{P}_{\boldsymbol{x}}^{-}(k)$. Denote sigma points as $\tilde{\boldsymbol{x}}^{(i)}$:

$$\hat{\boldsymbol{x}}^{(i)}(k) = \hat{\boldsymbol{x}}^{+}(k-1) + \tilde{\boldsymbol{x}}^{(i)}, \qquad i = 1,2,\cdots,2 \cdot N \tag{43}$$

$$\tilde{\boldsymbol{x}}^{(i)} = \left(\sqrt{N \cdot \boldsymbol{P}_{\boldsymbol{x}}^{+}(k-1)}\right)_i^T, \quad i = 1,2,\cdots,N$$
$$\tilde{\boldsymbol{x}}^{(i+N)} = -\left(\sqrt{N \cdot \boldsymbol{P}_{\boldsymbol{x}}^{+}(k-1)}\right)_i^T, \quad i = 1,2,\cdots,N \tag{44}$$

$$\hat{\boldsymbol{x}}^{-}(k) = \frac{1}{2N}\sum_{i=1}^{2N} f(\hat{\boldsymbol{x}}^{(\boldsymbol{i})}(k), \boldsymbol{0}, \boldsymbol{0}) \tag{45}$$

$$\boldsymbol{P}_{\boldsymbol{x}}^{-}(k) = \frac{1}{2N}\sum_{i=1}^{2N}\left(\hat{\boldsymbol{x}}^{(i)}(k) - \hat{\boldsymbol{x}}^{-}(k)\right)\left(\hat{\boldsymbol{x}}^{(i)}(k) - \hat{\boldsymbol{x}}^{-}(k)\right)^T + \boldsymbol{Q} \tag{46}$$

Second, estimate measurement output $\hat{\boldsymbol{y}}(k)$, measurement covariance $\boldsymbol{P}_{\boldsymbol{y}}(k)$ and cross covariance $\boldsymbol{P}_{\boldsymbol{xy}}(k)$:

$$\hat{\boldsymbol{y}}^{(i)}(k) = h(\hat{\boldsymbol{x}}^{(i)}(k), \boldsymbol{0}) \tag{47}$$

$$\hat{\boldsymbol{y}}(k) = \frac{1}{2N}\sum_{i=1}^{2N}\hat{\boldsymbol{y}}^{(i)}(k) \tag{48}$$

$$\boldsymbol{P}_{\boldsymbol{y}}(k) = \frac{1}{2N}\sum_{i=1}^{2N}\left(\hat{\boldsymbol{y}}^{(i)}(k) - \hat{\boldsymbol{y}}^{-}(k)\right)\left(\hat{\boldsymbol{y}}^{(i)}(k) - \hat{\boldsymbol{y}}^{-}(k)\right)^T + \boldsymbol{R} \tag{49}$$

$$\boldsymbol{P}_{\boldsymbol{xy}}(k) = \frac{1}{2N}\sum_{i=1}^{2N}\left(\hat{\boldsymbol{x}}^{(i)}(k) - \hat{\boldsymbol{x}}^{-}(k)\right)\left(\hat{\boldsymbol{y}}^{(i)}(k) - \hat{\boldsymbol{y}}^{-}(k)\right)^T \tag{50}$$

Lastly, calculate observer gain $K(k)$, a posteriori state estimation $\hat{x}^{+}(k)$ and covariance $P_x^{+}(k)$:

$$\boldsymbol{K}(k) = \boldsymbol{P}_{\boldsymbol{xy}}\boldsymbol{P}_{\boldsymbol{y}}^{-1} \tag{51}$$
$$\hat{\boldsymbol{x}}^{+}(k) = \hat{\boldsymbol{x}}^{-}(k) + \boldsymbol{K}(k)(\boldsymbol{y}(k) - \hat{\boldsymbol{y}}(k)) \tag{52}$$
$$\boldsymbol{P}_{\boldsymbol{x}}^{+}(k) = \boldsymbol{P}_{\boldsymbol{x}}^{-}(k) - \boldsymbol{K}(k)\boldsymbol{P}_{\boldsymbol{y}}(k)\boldsymbol{K}(k) \tag{53}$$

All the covariance matrices of the UKF are designed based on confidence level of measurement and traffic states, and referred to [3,28]. Initial guess of states are constant free driving density and flow speed at speed limit. All model parameters are calibrated based on the traffic scenario. Also, the estimated states are bounded to avoid negative density and flow speed.

2.4. Predict the arrival time at merging zone

After updating the state estimation using measurement from CAVs, future traffic states are predicted by propagating the traffic flow model forward in time. For each time instance k, the current state estimation $\hat{\boldsymbol{x}}^{+}(k)$ is used as the initial state for the propagation. The arrival time at the merging zone is predicted for every human-driven vehicle. Since for every time instance, the desired future speed of all CAVs are determined by the merging controller. These speed profiles can be considered as 'measurement' of future states to improve the accuracy of the traffic prediction. Note that the merging controller is implemented in a rolling horizon fashion and the desired speed of CAVs is updated at each control time step. Thus, the desired future speed will not be the same as the actual speed. Nevertheless, this desired future speed can provide a reasonable estimate of the actual speed and improve the prediction accuracy of the arrival time. The procedure is as the following:

1) The initial location and speed of each human-driven vehicle is known at each prediction update instance. Assume the current time instance is k and denote the location and speed of the i-th human-driven vehicle as $d_i(k)$ and $v_i(k)$. Denote the initial states estimation as $\hat{\boldsymbol{x}}^{+}(k)$.

2) By doing a numerical integration, the location of this vehicle at the next time instance can be obtained as $d_i(k+1) = d_i(k) + \mathrm{d}t \cdot v_i(k)$.

3) The state estimation is updated using the observer designed in Section 2.3. The measurement comes from the desired future speed of CAVs at time instance $k+1$. The updated states estimation is $\hat{\boldsymbol{x}}^{+}(k+1)$.

4) The speed of this vehicle at this next time step $v_i(k+1)$ is found by interpolating the traffic speed of the two adjacent cells to the location $d_i(k+1)$, using the states estimation $\hat{\boldsymbol{x}}^{+}(k+1)$.

5) The above process is repeated until the predicted vehicle trajectory arrives at the merging zone. The time difference between the time of arrival at the merging zone and the initial time is the predicted arrival time for this human-driven vehicle.

The above procedure is repeated for all human-driven vehicles within the control zone. Then the traffic states estimation gets updated again using measurement from CAVs and the predicted arrival time is updated again.

3. RESULTS AND DISCUSSION

3.1. Scenario

A single-lane secondary road merging onto a single-lane primary road scenario (see Figure 1)is simulated using the traffic simulator VISSIM and the proposed traffic prediction algorithm is used to estimate the arrival time to the merging zone of the human driven vehicles. The length of the control zone is selected as 400 meters and the length of the merging zone is 120 meters. The speed limit of the road is set to 50 km/h, the traffic flow input to the primary and secondary roads are set to 1200 veh/h and 900 veh/h respectively and the vehicles enter the simulated network following VISSIM's default stochastic time distribution. In VISSIM, the human-driven vehicles are simulated using the Wiedemann's car-following model. When CAVs enter the control zone, the merging coordination controller will determine their arrival time at the merging zone and control the desired speed. Once CAVs enter the merging zone, the merging controller will disengage. The lane-changing of CAVs within the merging zone are simulated using VISSIM's lane-change model.

To focus on evaluating the performance of the traffic prediction, the merging controller [9] is applied to control CAVs and the traffic scenario is simulated in VISSIM. The vehicle speed and location information is stored and used as input to the traffic prediction algorithm. A total of nine penetration rates are assessed ranging from 10% to 90%. The penetration rate refers to the percentage of CAVs among all vehicles in the simulated traffic scenario. Each penetration rate scenario is simulated for 500 seconds which corresponds to about total of 300 vehicles entering the merging area (including both CAVs and human-

driven vehicles). Note that only the arrival time of the human-driven vehicles is predicted since the merging controller will control the arrival time of all CAVs. This means that for 10% penetration rate, the algorithm predicts the arrival time of about 270 vehicles, while for 90% penetration rate, the arrival time of about 30 vehicles is predicted. The baseline scenario to assess the performance of the prediction is selected as the scenario in which the arrival time for human-driven vehicles is estimated assuming they follow a constant speed [17].

In this work, the traffic prediction of the arrival time is not yet feedbacked to the merging controller, which is left for future work. The arrival time is compared for different penetration rate scenarios with respect to the baseline to understand and evaluate the performance of the proposed traffic prediction algorithm.

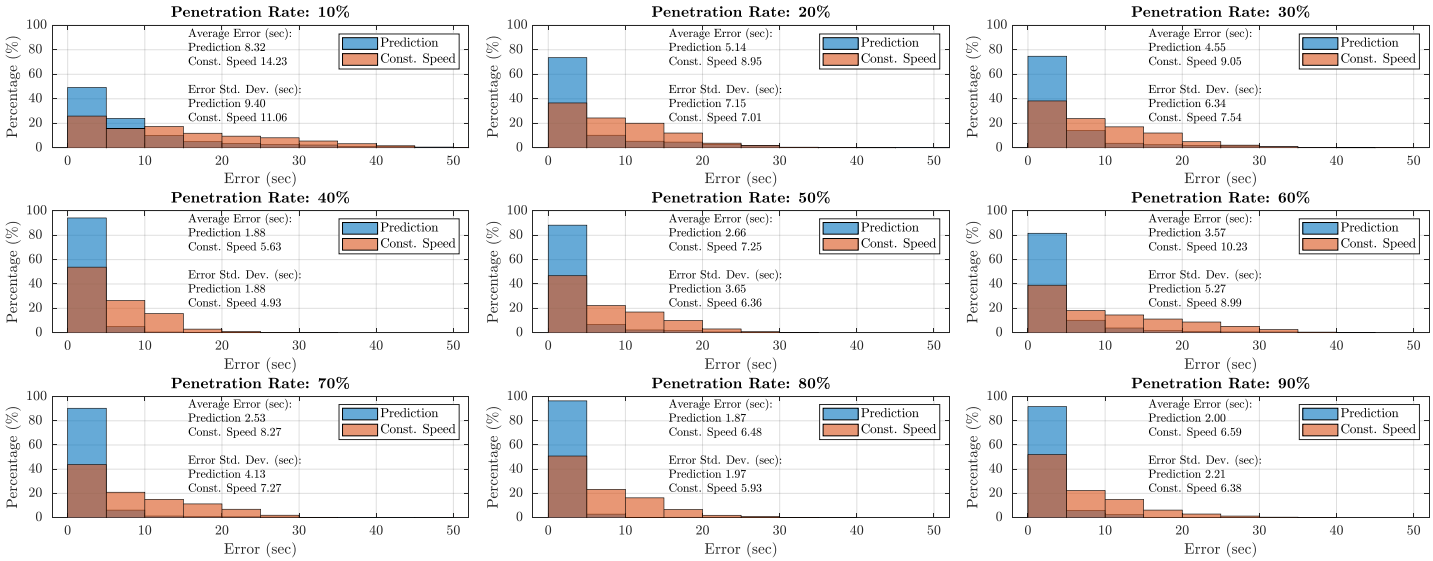

Figure 3 Arrival time prediction error comparison between traffic prediction and constant speed assumption

3.2. Results

Figure 3 shows the histograms for the arrival time estimation error between the proposed traffic prediction algorithm and the constant speed assumption. Since the merging coordination control is updated in a rolling horizon fashion, the arrival time prediction for each vehicle is updated at every control time step. This means that, even for a single vehicle, multiple predictions on the arrival time are conducted by the traffic prediction algorithm. For example, if it takes 20 seconds for a human-driven vehicle to cross the control zone, there will be total of 20/0.5=40 predictions (as the update time of the prediction is set to 0.5 seconds in Section 2). For each of these 40 predictions, the error between the predicted and actual arrival time is calculated, and this procedure is repeated for all human-driven vehicles under the same penetration rate. After that, the histogram is plotted for all prediction errors of all these vehicles. The y-axis of each histogram is normalized to show the percentage of each case with respect to the total number of predictions. This is because scenarios of different penetration rates have different numbers of human-driven vehicles and hence the numbers of predictions. In general, it can be seen that the average error on arrival time prediction is significantly reduced using the proposed traffic prediction algorithm comparing to the constant speed assumption. The histograms also show that the errors of the proposed prediction algorithm are more 'aggregated', means that both the standard deviations and the maximum prediction errors are significantly reduced. The values of standard deviation for each penetration rate are shown as the texts on each subfigure.

As shown in Figure 4, in most penetration rates, the proposed traffic prediction can achieve more than 50% reduction in errors of arrival time estimation, comparing to the constant speed assumption. Figure 4 also shows that, in general, the arrival time errors of both the proposed prediction algorithm and the constant speed assumption is significantly decreased with higher penetration rates. This makes sense since it is anticipated that the traffic flow is mostly smoothed with high penetration rates of CAVs. The arrival time is not monotonically decreasing as the penetration rate increases, especially when there are about the same amount of CAVs and human-driven vehicles on the road (40%-60% penetration rates). This is because in these scenarios, the prediction errors depend on the relative positions of CAVs and human-driven vehicles. If several CAVs are following each other, then the traffic flow after these CAVs will be smoothed out as well. The human-driven vehicles following these CAVs will benefit and have smoothed speed profiles. In these cases, the traffic prediction can make a more accurate prediction on arrival time. If CAVs are scattered and there will always be human-driven vehicles in between CAVs, then the effectiveness of traffic flow smoothing will be limited. This is because in these scenarios the current merging controller does

not have an accurate estimation on the behaviors of human-driven vehicles. The different behaviors of human-driven vehicles and CAVs will bring in 'disturbances' to the control of CAVs. As a result, the controller may have to adjust the arrival sequence and desired of CAVs frequently, which causes the errors in traffic prediction. Figure 5 shows the spatio-temporal traffic speed plot for the 60% penetration rate scenario as an example. It can be seen that the predicted flow speed has reasonable accuracy comparing to the actual flow speed of the VISSIM simulation, which validates the proposed traffic prediction algorithm.

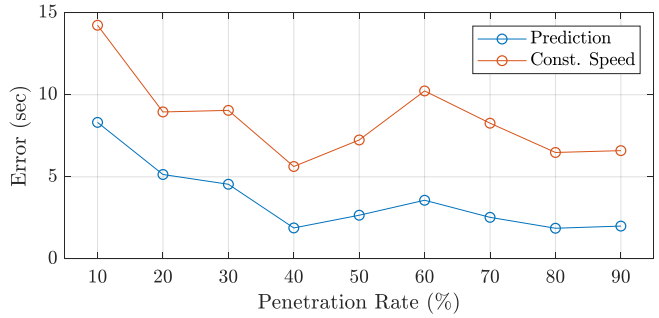

Figure 4 Average arrival time prediction error comparison between traffic prediction and constant speed assumption

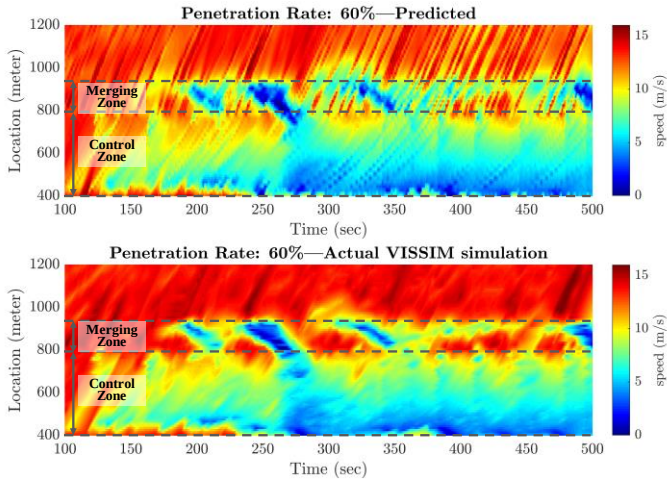

Figure 5 Spatio-temporal states comparison between predicted flow speed and actual flow speed of VISSIM simulation

4. CONCLUSION

In this work, a traffic prediction algorithm is developed for a merging coordination application under mixed traffic. The merging controller coordinates the arrival sequence and speed of CAVs to maximize the energy efficiency and mobility. The controller receives information from CAVs but not the human-driven vehicles. The integration of a traffic prediction with the merging coordination control can potentially improve the performance under mixed traffic conditions. The performance of the developed traffic prediction algorithm is investigated for various penetration rates of connectivity for a single-lane secondary road merging to a single-lane primary road. The results show that, comparing to a constant speed assumption of human-driven vehicles, the proposed traffic prediction algorithm can reduce the arrival time prediction error by more than 50%. Future work includes the integration of the traffic prediction with the merging coordination control and evaluation of its performance, applying the traffic prediction to multi-lane merging scenarios, and experimental validation.

ACKNOWLEDGEMENTS

The work described was sponsored in part by the U.S. Department of Energy (DOE) Vehicle Technologies Office (VTO) under the Systems and Modeling for Accelerated Research in Transportation (SMART) Mobility Laboratory Consortium, an initiative of the Energy Efficient Mobility Systems (EEMS) Program and in part by the Energy and Transportation Science Division, Oak Ridge National Laboratory.

REFERENCES

[1] United States Department of Transportation, 2015, "Connected Vehicle Applications" [Online]. Available: https://www.its.dot.gov/pilots/cv_pilot_apps.htm. [Accessed: 14-Aug-2018].

[2] Mahler, G., and Vahidi, A., 2014, "An Optimal Velocity-Planning Scheme for Vehicle Energy Efficiency through Probabilistic Prediction of Traffic-Signal Timing," IEEE Trans. Intell. Transp. Syst., **15**(6), pp. 2516–2523.

[3] Shao, Y., and Sun, Z., 2020, "Eco-Approach With Traffic Prediction and Experimental Validation for Connected and Autonomous Vehicles," IEEE Trans. Intell. Transp. Syst.

[4] Moser, D., Schmied, R., Waschl, H., Del Re, L., and Re, L. del, 2018, "Flexible Spacing Adaptive Cruise Control Using Stochastic Model Predictive Control," IEEE Trans. Control Syst. Technol., **26**(1), pp. 114–127.

[5] Guanetti, J., Kim, Y., and Borrelli, F., 2018, "Control of Connected and Automated Vehicles: State of the Art and Future Challenges," Annu. Rev. Control, **45**, pp. 18–40.

[6] Hu, J., Shao, Y., Sun, Z., Wang, M., Bared, J., and Huang, P., 2016, "Integrated Optimal Eco-Driving on Rolling Terrain for Hybrid Electric Vehicle with Vehicle-Infrastructure Communication," Transp. Res. Part C Emerg. Technol., **68**, pp. 228–244.

[7] Homchaudhuri, B., Vahidi, A., and Pisu, P., 2017, "Fast Model Predictive Control-Based Fuel Efficient Control Strategy for a Group of Connected Vehicles in Urban Road Conditions," IEEE Trans. Control Syst. Technol., **25**(2), pp. 760–767.

[8] Altan, O. D., Wu, G., Barth, M. J., Boriboonsomsin, K., and Stark, J. A., 2017, "GlidePath: Eco-Friendly Automated Approach and Departure at Signalized Intersections," IEEE Trans. Intell. Veh., **2**(4), pp. 266–277.

[9] Rios-Torres, J., and Malikopoulos, A. A., 2017, "Automated and Cooperative Vehicle Merging at

Highway On-Ramps," IEEE Trans. Intell. Transp. Syst., **18**(4), pp. 780–789.

[10] Moser, D., Waschl, H., Schmied, R., Efendic, H., and del Re, L., 2015, "Short Term Prediction of a Vehicle's Velocity Trajectory Using ITS," SAE Int. J. Passeng. Cars - Electron. Electr. Syst., **8**(2), pp. 364–370.

[11] Liu, K., Asher, Z., Gong, X., Huang, M., and Kolmanovsky, I., 2019, "Vehicle Velocity Prediction and Energy Management Strategy Part 1: Deterministic and Stochastic Vehicle Velocity Prediction Using Machine Learning," *SAE Technical Papers*, SAE International.

[12] Carvalho, A., Lefévre, S., Schildbach, G., Kong, J., and Borrelli, F., 2015, "Automated Driving: The Role of Forecasts and Uncertainty - A Control Perspective," Eur. J. Control, **24**, pp. 14–32.

[13] Jiang, H., Hu, J., An, S., Wang, M., and Park, B. B., 2017, "Eco Approaching at an Isolated Signalized Intersection under Partially Connected and Automated Vehicles Environment," Transp. Res. Part C Emerg. Technol., **79**, pp. 290–307.

[14] Hyeon, E., Kim, Y., Prakash, N., and Stefanopoulou, A. G., 2019, "Short-Term Speed Forecasting Using Vehicle Wireless Communications," *2019 American Control Conference (ACC)*, Philadelphia, PA, pp. 736–741.

[15] Litman, T. A., 2015, "Autonomous Vehicle Implementation Predictions," Victoria, Canada Victoria Transp. Policy Institute.

[16] Feng, Y., Head, K. L., Khoshmagham, S., and Zamanipour, M., 2015, "A Real-Time Adaptive Signal Control in a Connected Vehicle Environment," Transp. Res. Part C Emerg. Technol., **55**, pp. 460–473.

[17] Rios-Torres, J., and Malikopoulos, A. A., 2018, "Impact of Partial Penetrations of Connected and Automated Vehicles on Fuel Consumption and Traffic Flow," IEEE Trans. Intell. Veh., **3**(4), pp. 453–462.

[18] Arvin, R., Kamrani, M., Khattak, A. J., and Rios-Torres, J., 2018, "Safety Impacts of Automated Vehicles in Mixed Traffic," *Transportation Research Board 97th Annual Meeting*.

[19] Treiber, M., and Kesting, A., 2013, *Traffic Flow Dynamics*, Springer Berlin Heidelberg, Berlin, Heidelberg.

[20] Panwai, S., and Dia, H., 2005, "Comparative Evaluation of Microscopic Car-Following Behavior," IEEE Trans. Intell. Transp. Syst., **6**(3), pp. 314–325.

[21] Lighthill, M. J., and Whitham, G. B., 1955, "On Kinematic Waves II. A Theory of Traffic Flow on Long Crowded Roads," Proc. R. Soc. London. Ser. A. Math. Phys. Sci., **229**(1178), pp. 317–345.

[22] Payne, H. J., 1971, "Models of Freeway Traffic and Control," *Mathematical Models of Public Systems*, La Jolla, Calif., Simulation Councils, pp. 55–61.

[23] Wang, R., Work, D. B., Sowers, R., Member, S., Work, D. B., and Sowers, R., 2016, "Multiple Model Particle Filter for Traffic Estimation and Incident Detection," IEEE Trans. Intell. Transp. Syst., **17**(12), pp. 1–10.

[24] Yuan, Y., Van Lint, J. W. C., Wilson, R. E., Van Wageningen-Kessels, F., and Hoogendoorn, S. P., 2012, "Real-Time Lagrangian Traffic State Estimator for Freeways," IEEE Trans. Intell. Transp. Syst., **13**(1), pp. 59–70.

[25] Lv, Y., Duan, Y., Kang, W., Li, Z., and Wang, F. Y., 2015, "Traffic Flow Prediction with Big Data: A Deep Learning Approach," IEEE Trans. Intell. Transp. Syst., **16**(2), pp. 865–873.

[26] Zhang, F., Xi, J., and Langari, R., 2017, "Real-Time Energy Management Strategy Based on Velocity Forecasts Using V2V and V2I Communications," IEEE Trans. Intell. Transp. Syst., **18**(2), pp. 416–430.

[27] Ye, F., Hao, P., Qi, X., Wu, G., Boriboonsomsin, K., and Barth, M. J., 2019, "Prediction-Based Eco-Approach and Departure at Signalized Intersections with Speed Forecasting on Preceding Vehicles," IEEE Trans. Intell. Transp. Syst., **20**(4), pp. 1378–1389.

[28] Wang, Y., and Papageorgiou, M., 2005, "Real-Time Freeway Traffic State Estimation Based on Extended Kalman Filter: A General Approach," Transp. Res. Part B Methodol., **39**(2), pp. 141–167.

[29] Zemouche, A., Rajamani, R., Phanomchoeng, G., Boulkroune, B., Rafaralahy, H., and Zasadzinski, M., 2017, "Circle Criterion-Based $\mathscr{H}\infty$observer Design for Lipschitz and Monotonic Nonlinear Systems – Enhanced LMI Conditions and Constructive Discussions," Automatica, **85**, pp. 412–425.

[30] Nugroho, S. A., Taha, A. F., and Claudel, C., 2019, "Traffic Density Modeling and Estimation on Stretched Highways: The Case for Lipschitz-Based Observers," *Proceedings of the American Control Conference*, Institute of Electrical and Electronics Engineers Inc., pp. 2658–2663.

[31] Simon, D., 2006, *Optimal State Estimation: Kalman, H∞, and Nonlinear Approaches*, John Wiley & Sons, Inc.

[32] Wan, E. A., and Van Der Merwe, R., 2000, "The Unscented Kalman Filter for Nonlinear Estimation," *IEEE 2000 Adaptive Systems for Signal Processing, Communications, and Control Symposium*, pp. 153–158.

[33] Suh, B., Shao, Y., and Sun, Z., 2020, "Vehicle Speed Prediction for Connected and Autonomous Vehicles Using Communication and Perception," *2020 American Control Conference (ACC)*.